Article

Relativistic Effects on Satellite–Ground Two–Way Precise Time Synchronization

Yanming Guo [1,2,3] iD **, Yan Bai** [2,3,*] **, Shuaihe Gao** [1,*] **, Zhibing Pan** [1] **, Zibin Han** [1,2,3] **, Decai Zou** [1,2,3] **, Xiaochun Lu** [1,2,3] **and Shougang Zhang** [1,2,3]

1   National Time Service Center, Chinese Academy of Sciences, Xi'an 710600, China;
     guoyanming@ntsc.ac.cn (Y.G.); panzhibing@ntsc.ac.cn (Z.P.); hanzibin@ntsc.ac.cn (Z.H.);
     zoudecai@ntsc.ac.cn (D.Z.); luxc@ntsc.ac.cn (X.L.); zhangshougang@ntsc.ac.cn (S.Z.)
2   University of Chinese Academy of Sciences, Beijing 100039, China
3   Key Laboratory of Precise Positioning and Timing Technology, Xi'an 710600, China
*   Correspondence: by@ntsc.ac.cn (Y.B.); gaoshuaihe@ntsc.ac.cn (S.G.)

Abstract: An ultrahigh precise clock (space optical clock) will be installed onboard a low-orbit spacecraft (a usual expression for a low-orbit satellite operating on an orbit at an altitude of less than 1000 km) in the future, which will be expected to obtain better time-frequency performance in a microgravity environment, and provide the possible realization of ultrahigh precise long-range time synchronization. The advancement of the microwave two-way time synchronization method can offer an effective solution for developing time-frequency transfer technology. In this study, we focus on a method of precise satellite-ground two-way time synchronization and present their key aspects. For reducing the relativistic effects on two-way precise time synchronization, we propose a high-precision correction method. We show the results of tests using simulated data with fully realistic effects such as atmospheric delays, orbit errors, and earth gravity, and demonstrate the satisfactory performance of the methods. The accuracy of the relativistic error correction method is investigated in terms of the spacecraft attitude error, phase center calibration error (the residual error after calibrating phase center offset), and precise orbit determination (POD) error. The results show that the phase center calibration error and POD error contribute greatly to the residual of relativistic correction, at approximately 0.1~0.3 ps, and time synchronization accuracy better than 0.6 ps can be achieved with our proposed methods. In conclusion, the relativistic error correction method is effective, and the satellite-ground two-way precise time synchronization method yields more accurate results. The results of Beidou two-way time synchronization system can only achieve sub-ns accuracy, while the final accuracy obtained by the methods in this paper can improved to ps-level.

Keywords: clock; microgravity environment; microwave; two-way time synchronization; relativistic; performance

1. Introduction

The invention of atomic clocks provides an effective time solution for precision positioning, navigation, and timing (PNT) [1]. The atomic clock is known to be the heart of the global navigation satellite system (GNSS). High-precision time-frequency transfer technology can be achieved through the time comparison algorithm of satellite-satellite, satellite-ground, ground-ground, or other communication links. At present, microwave two-way time synchronization technology is one of the most accurate time-frequency transfer methods. In a BeiDou-3 navigation system (BDS-3) time synchronization experiment, it was shown that the time synchronization accuracy can reach the sub-ns level [2,3], which is limited by the accuracy of the onboard atomic clocks onboard. To further improve the accuracy, the European Space Agency (ESA) proposed a novel idea to enhance the performance of time synchronization. To operate a new generation payload with a high-precision atomic clock ensemble (with a stability better than 1E-16@1day) onboard the International

Space Station (ISS) in a microgravity environment, ultrahigh precise two-way time synchronization was achieved through a microwave link (MWL). The results showed that the time synchronization accuracy is expected to be less than 10 ps when using a multifrequency two-way time synchronization algorithm [4–7]. China also plans to deploy high-precision atomic clocks (including space optical clocks with a stability better than 1E-17@1day) on the Chinese Space Station (CSS) to develop an ultrahigh precise time reference in space to further improve two-way time synchronization accuracy [8].

The relativistic effect affects the time synchronization performance of satellite-ground links (GSLs) or inter-satellite links (ISLs), especially for spacecraft operating in low orbits, e.g., ISS, CSS, low-orbit earth orbit (LEO) satellites, etc. The relativistic effect can be more negative due to its high-speed motion (nearly 7 km/s) [9,10]. This research focuses on a high-precision time synchronization method, which depends on the two-way links between ground stations and low-orbit satellites equipped with high-precision atomic clocks. Considering the complicated space environment of spacecrafts in low-orbit, we introduce a variety of errors to generate the simulation data. On this basis, we describe the relativistic effects and deduce the correction methods. To validate the methods, we analyze the impact of different orbital errors (including attitude error, phase center calibration error, and precise orbit determination error) on the relativistic effects, and derive the final results of satellite-ground two-way time synchronization. Finally, some conclusions are offered.

2. Two-Way Time Synchronization Method with GSLs

The Beidou (BD) Ka-band inter-satellite link (ISL) system employs a time division multiple access (TDMA) communication mode to realize two-way time synchronization with GSLs or ISLs, and the TDMA mode limits the observations of each pass over a given ground station [11]. To increase the GSL observations in the duration of each pass (300–400 s), the improved method (see Figure 1) deploys a communication mode of simultaneous transmission or simultaneous reception of signals [12], as shown in Figure 1. GSLs are composed of satellite-ground ranging pairs, including uplink pseudorange observations and downlink pseudorange observations. Assuming that satellite B receives an uplink signal with an f1 frequency (Ka-band, 20~40 GHz) from ground station A at its local time T_0, the uplink pseudorange observation ($\rho_{AB}(T_0)$) can be obtained. Similarly, ground station A receives two downlink signals with an f2 frequency and f3 frequency (Ka-band, 20~40 GHz) from satellite B at its local time T_0, and the downlink pseudorange observation ($\rho_{BA}(T_0)$) can be obtained. The f2 and f3 frequency signals are mainly used to correct the atmospheric delay. And the f1 and f2 frequency signals are mainly used to perform new method of two-way time synchronization, referring to Two-way Satellite Time and Frequency Transfer (TWSTFT) [13]. For specific description, according to the pair links of f1 and f2, $\rho_{AB}(T_0)$ and $\rho_{BA}(T_0)$ can be written as:

$$
\begin{aligned}
\rho_{AB}(T_0) = {} & \left|\mathbf{X}_B(T_0) - \mathbf{X}_A(T_0 - \tfrac{\rho_{AB}}{c})\right| + c \cdot \left[x_B(T_0) - x_A(T_0 - \tfrac{\rho_{AB}}{c})\right] \\
& + c \cdot \left(\delta_A^{Snd} + \delta_B^{Rcv}\right) + c \cdot \delta_{AB}^{tro}(T_0 - \tfrac{\rho_{AB}}{c}, T_0) + c \cdot \delta_{AB}^{ion}(T_0 - \tfrac{\rho_{AB}}{c}, T_0) \\
& + c \cdot \delta_{AB}^{rel}(T_0 - \tfrac{\rho_{AB}}{c}, T_0) + c \cdot \delta_{AB}^{grav}(T_0 - \tfrac{\rho_{AB}}{c}, T_0) + \varepsilon_{AB}
\end{aligned}
\tag{1}
$$

and

$$
\begin{aligned}
\rho_{BA}(T_0) = {} & \left|\mathbf{X}_A(T_0) - \mathbf{X}_B(T_0 - \tfrac{\rho_{BA}}{c})\right| + c \cdot \left[x_A(T_0) - x_B(T_0 - \tfrac{\rho_{BA}}{c})\right] \\
& + c \cdot \left(\delta_B^{Snd} + \delta_A^{Rcv}\right) + c \cdot \delta_{BA}^{tro}(T_0 - \tfrac{\rho_{BA}}{c}, T_0) + c \cdot \delta_{BA}^{ion}(T_0 - \tfrac{\rho_{BA}}{c}, T_0) \\
& + c \cdot \delta_{BA}^{rel}(T_0 - \tfrac{\rho_{BA}}{c}, T_0) + c \cdot \delta_{BA}^{grav}(T_0 - \tfrac{\rho_{BA}}{c}, T_0) + \varepsilon_{BA}
\end{aligned}
\tag{2}
$$

where c is the speed of light, $\mathbf{X}_A$ and $\mathbf{X}_B$ are the position vectors of ground station A and satellite B (the positions of the ground station and the spcacecraft orbitography are expressed in the earth-centered inertial (ECI) reference frame), x_A and x_B are the clock errors of ground station A and satellite B, δ_{AB}^{tro} and δ_{BA}^{tro} are the tropospheric delays of the uplink path and downlink path, δ_{AB}^{ion} and δ_{BA}^{ion} are the ionospheric delays of the uplink path

and downlink path, δ_{AB}^{rel} and δ_{BA}^{rel} are the periodic relativity delays of the uplink path and downlink path, δ_{AB}^{grav} and δ_{BA}^{grav} are the gravitational errors of signals, δ^{Snd} and δ^{Rcv} are the transmission and reception delays of the payload, and ε includes phase center offset (PCO) and unknown errors.
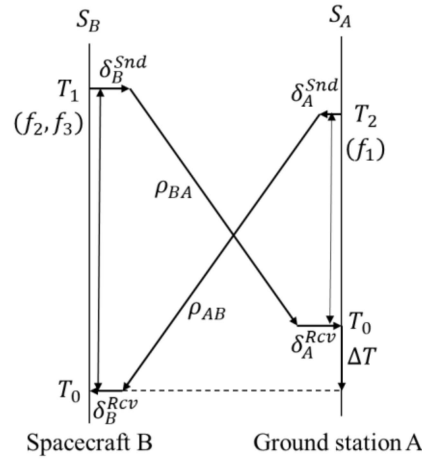

Figure 1. The principle of the two-way time synchronization method with GSLs.

Furthermore, the subtraction of $\rho_{AB}(T_0)$ and $\rho_{BA}(T_0)$ forms a geometry-free observable [14] and is typically used for estimating satellite clock errors, as follows:
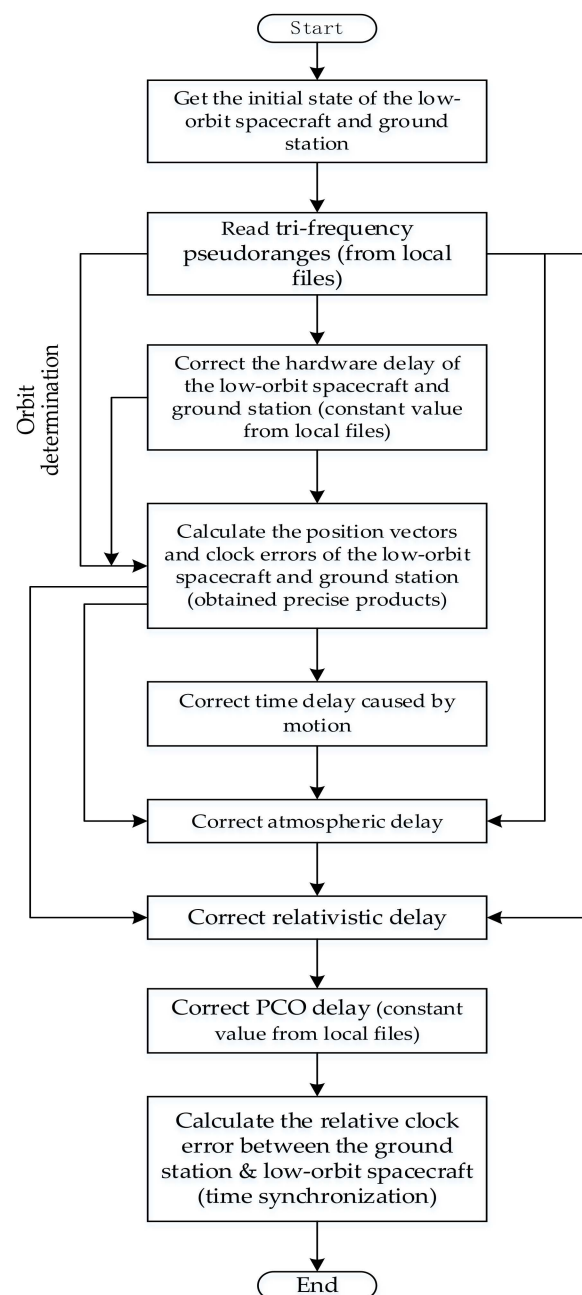
$$
\begin{aligned}
\Delta T(T_0) =\ & x_B(T_0) - x_A(T_0) \\
=\ & \frac{\rho_{AB}(T_0) - \rho_{BA}(T_0)}{c} - \left(x_B\!\left(T_0 - \frac{\rho_{BA}}{c}\right) - x_A\!\left(T_0 - \frac{\rho_{AB}}{c}\right) \right) \\
& - \left(\left| \mathbf{X}_B(T_0) - \mathbf{X}_A\!\left(T_0 - \frac{\rho_{AB}}{c}\right) \right| - \left| \mathbf{X}_A(T_0) - \mathbf{X}_B\!\left(T_0 - \frac{\rho_{BA}}{c}\right) \right| \right) / c \\
& - \left(\delta_{AB}^{tro}\!\left(T_0 - \frac{\rho_{AB}}{c}, T_0\right) - \delta_{BA}^{tro}\!\left(T_0 - \frac{\rho_{BA}}{c}, T_0\right) \right) \\
& - \left(\delta_{AB}^{ion}\!\left(T_0 - \frac{\rho_{AB}}{c}, T_0\right) - \delta_{BA}^{ion}\!\left(T_0 - \frac{\rho_{BA}}{c}, T_0\right) \right) \\
& - \left(\delta_{AB}^{rel}\!\left(T_0 - \frac{\rho_{AB}}{c}, T_0\right) - \delta_{BA}^{rel}\!\left(T_0 - \frac{\rho_{BA}}{c}, T_0\right) \right) \\
& - \left(\delta_{AB}^{grav}\!\left(T_0 - \frac{\rho_{AB}}{c}, T_0\right) - \delta_{BA}^{grav}\!\left(T_0 - \frac{\rho_{BA}}{c}, T_0\right) \right) \\
& - \left(\left(\delta_A^{Rcv} + \delta_B^{Snd} \right) - \left(\delta_B^{Rcv} + \delta_A^{Snd} \right) \right) - \left(\varepsilon_{AB} - \varepsilon_{BA} \right)
\end{aligned}
\tag{3}
$$

From Equation (3), for precise time synchronization, the decoupling of relative clock error ΔT relates to the correction models of time delay caused by motion, tropospheric delay, ionospheric delay, relativistic delay, hardware delay, PCO delay, etc. The detailed process of the two-way time synchronization method is shown in Figure 2.

Specifically, the hardware delay can be considered as a constant that can be accurately deducted. The time delay caused by motion, atmospheric delay, relativistic delay, and PCO delay can be calibrated by precise models. Table 1 shows the detailed error correction strategies.

Table 1. Error correction strategies for the two-way time synchronization process.

Item	Strategy
Time delay caused by motion	Precise model (With precise orbit and clock products) [15]
Atmospheric delay (Tropospheric delay and ionospheric delays)	Precise model [16,17]
Relativistic delay	Corrected by precise model
Hardware delay	Considering as a constant value over several days [18]
PCO delay	Calibrated: provide by manufacturer values for antennas [19]

```
                    ┌─────────┐
                    │  Start  │
                    └─────────┘
                         │
         ┌───────────────────────────────┐
         │ Get the initial state of the low-
         │  orbit spacecraft and ground
         │           station             │
         └───────────────────────────────┘
                         │
         ┌───────────────────────────────┐
         │      Read tri-frequency        │
         │  pseudoranges (from local      │
         │           files)               │
         └───────────────────────────────┘
                         │
         ┌───────────────────────────────┐
         │   Correct the hardware delay of│
         │  the low-orbit spacecraft and  │
         │ ground station (constant value │
         │        from local files)       │
         └───────────────────────────────┘
                         │
         ┌───────────────────────────────┐
         │ Calculate the position vectors │
         │  and clock errors of the low-orbit
         │   spacecraft and ground station│
         │  (obtained precise products)   │
         └───────────────────────────────┘
                         │
         ┌───────────────────────────────┐
         │   Correct time delay caused by │
         │            motion              │
         └───────────────────────────────┘
                         │
         ┌───────────────────────────────┐
         │     Correct atmospheric delay  │
         └───────────────────────────────┘
                         │
         ┌───────────────────────────────┐
         │     Correct relativistic delay │
         └───────────────────────────────┘
                         │
         ┌───────────────────────────────┐
         │  Correct PCO delay (constant   │
         │    value from local files)     │
         └───────────────────────────────┘
                         │
         ┌───────────────────────────────┐
         │   Calculate the relative clock │
         │    error between the ground    │
         │ station & low-orbit spacecraft │
         │     (time synchronization)     │
         └───────────────────────────────┘
                         │
                    ┌─────────┐
                    │   End   │
                    └─────────┘
```

Orbit determination

Figure 2. The detailed process of the two-way time synchronization (step-by-step).

For ps-level time synchronization, the error factors of tropospheric delay, relativistic delay, and time delay caused by motion must be considered. The time delay caused by motion can be precisely estimated by precise orbit and clock products (the accuracy of the orbit is better than 10 cm), and the results show that the correction accuracy is better than 0.02 ps [20]. To reduce the effect of tropospheric delay, we adopt a precise model, with data from a microwave radiometer. In addition, the correction of the relativistic effect is a significant factor to improve the accuracy of satellite-ground time synchronization.

3. Relativistic Effects and Corrections

According to the theory of relativity, the simultaneity of spatially separated events is not absolute. The relativistic errors in the satellite-ground two-way time synchronization algorithm are mainly caused by the high-speed relative motion between the low-orbit spacecraft and the ground station. This section mainly introduces relativistic errors and

derives error correction methods. The main relativistic effects on satellite-ground two-way precise time synchronization operations are as follows [21–23]:

- Relativistic effect on frequency (nominal frequency offset and periodic relativity delay)
- Relativistic path range effect (gravitational time delay)

3.1. Relativistic Effect on Frequency

The relativistic effect on frequency is caused by the relative movement (special relativity) and difference in gravity field (general relativity) between the low-orbit spacecraft and the ground station receiver. In the ECI coordinate frame, there is no Sagnac effect, and the ground station can be treated as an ultralow-orbit spacecraft. Thus, the relativistic effect on the frequency of the low-orbit spacecraft and ground station can be computed by

$$\Delta f^{rel\_f} = -\left[\frac{1}{2}\left(\frac{v}{c}\right)^2 + \frac{\Delta U}{c^2}\right] \cdot f \tag{4}$$

where Δf^{rel_f} is the relativistic effect on frequency, the v is the velocity of the target (low-orbit spacecraft or ground station in the ECI reference frame), ΔU is the earth potential difference between the target and object on the surface of the earth, and f is the nominal frequency.

A spacecraft orbiting the earth is in the gravitational field of the earth and is subjected to various perturbation forces. The perturbation force levels of different in-orbit spacecraft are shown in Table 2. The perturbation magnitude of nonspherical gravitation can reach 10^{-3}, which has an impact on the gravitational potential of objects. For the ps-level time synchronization method, it is also necessary to consider the effect of the earth's nonspherical perturbation force beside the gravity of the earth [24]. Thus, the potential differences between the target and object on the surface of the earth can be expressed as:

$$\Delta U = W_s - W_0 = \frac{GM}{r_s} - V - \frac{GM}{r_e} \tag{5}$$

where W is the earth potential, GM is the geocentric gravitational constant of the earth, r_e is the earth radius, r_s is the geocentric distance, and V is the nonspherical perturbation potential of earth.

Table 2. Level of perturbation forces on satellites in different orbits [25].

Type	Level of Perturbation Force						
	Nonspherical Gravitation		**Lunisolar Gravitation**		**Atmospheric Drag**	**Solar Radiation**	**Tidal**
	J_2	**Others**	**Sun**	**Moon**			
LEO	10^{-3}	$10^{-7} \sim 10^{-8}$	10^{-8}	10^{-7}	$10^{-6} \sim 10^{-10}$	10^{-8}	10^{-8}
MEO	10^{-4}	10^{-7}	1.8×10^{-6}	3.9×10^{-6}	$< 10^{-10}$	1.6×10^{-7}	10^{-9}
GEO	1.2×10^{-4}	10^{-7}	7.5×10^{-6}	1.6×10^{-5}	$< 10^{-10}$	4.0×10^{-7}	10^{-8}

According to the two-body problem [26], Equation (4) can be rewritten as

$$\begin{aligned}\Delta f^{rel-f} &= -\frac{f}{c^2}\left(\frac{2GM}{r_s} - \frac{GM}{r_e} - \frac{GM}{2a}\right) + \frac{f}{c^2} \cdot V \\ &= \frac{GM}{c^2}\left[\frac{1}{r_e} - \frac{3}{2a}\right] \cdot f - \frac{2f\sqrt{aGM}}{tc^2}e\sin E + \frac{f}{c^2} \cdot V\end{aligned} \tag{6}$$

where a is the semi-major axis, e is the eccentricity, and E is the eccentric anomaly.

The first term in Equation (6) represents the nominal frequency offset (NFO), which can be corrected by reducing the atomic clock frequency of spacecrafts or ground stations. In this way, a major part of the relativistic effects is removed. However, the temporal variations of the relativistic effects remain (periodic relativity delay), and they can be

eliminated by data post-processing. Furthermore, the periodic relativity delay of spacecraft i at time t can be expressed as:

$$\delta_i^{rel}(t) = -\frac{2\sqrt{aGM}}{c^2}e\sin E + \Delta\delta_{J2} + \Delta\delta_{other}\Big|_{i(t)} \tag{7}$$

in which

$$\begin{cases} \Delta\delta_{J2} + \Delta\delta_{other} = \frac{1}{c^2}\int V dt \\ V = \frac{GM}{r_s}\left[\sum_{l=2}^{\infty}\sum_{m=0}^{l}\left(\frac{a_E}{r_s}\right)^l P_{lm}(\sin\varphi)[C_{lm}cosm\lambda + S_{lm}sinm\lambda]\right] \end{cases} \tag{8}$$

where a_E is the semimajor axis of Earth's equator, φ is latitude, λ is longitude, and (C_{lm}, S_{lm}) are the coefficients of Earth's gravitational potential.

Therefore, according to Equations (3), (7) and (8), the periodic relativity delay on two-way time synchronization of GSLs can be corrected. The periodic relativity delay of two-way time synchronization can be expressed as:

$$\begin{aligned} \delta^{rel} &= \left(\delta_{AB}^{rel}(T_0 - \frac{\rho_{AB}}{c}, T_0) - \delta_{BA}^{rel}(T_0 - \frac{\rho_{BA}}{c}, T_0)\right) \\ &= \left(\Delta\delta_{J2} + \Delta\delta_{other} - \frac{2\sqrt{aGM}}{c^2}e\sin E\right)\Big|_{B(T_0)} \\ &\quad - \left(\Delta\delta_{J2} + \Delta\delta_{other} - \frac{2\sqrt{aGM}}{c^2}e\sin E\right)\Big|_{A(T_0 - \frac{\rho_{AB}}{c})} \\ &\quad + \left(\Delta\delta_{J2} + \delta_{other} - \frac{2\sqrt{aGM}}{c^2}e\sin E\right)\Big|_{B(T_0 - \frac{\rho_{BA}}{c})} \\ &\quad - \left(\Delta\delta_{J2} + \delta_{other} - \frac{2\sqrt{aGM}}{c^2}e\sin E\right)\Big|_{A(T_0)} \end{aligned} \tag{9}$$

3.2. Relativistic Path Range Effect

The relativistic path range effect is also known as the gravitational time delay of signals. Due to the impact of the gravity field, the paths of signals are not Euclidian straight lines. Therefore, the general relativity of signal transmission from target A at time t_1 to B at t_2 can be expressed by the Holdridge model [27], as follows:

$$\delta_{AB}^{grav}(t_1, t_2) = \frac{2GM}{c^3}ln\left(\frac{r_A(t_1) + r_B(t_2) + d_{AB}(t_1, t_2)}{r_A(t_1) + r_B(t_2) - d_{AB}(t_1, t_2)}\right) \tag{10}$$

where r is the geocentric distance, in which

$$d_{AB}(t_1, t_2) = |\mathbf{X}_B(t_2) - \mathbf{X}_A(t_1)| \tag{11}$$

The gravitational time delay correction model is considered in the ECI coordinate frame, and only considers the impact of gravity. The gravitational effects of the Moon, Sun, and other planets are reduced to tidal forces with very small relativistic corrections. Then, substituting Equation (9) into Equation (3) can precisely correct the gravitational time delay on two-way time synchronization.

Similar to the derivation of periodic relativity delay of two-way time synchronization from Equations (3) and (7)–(9), the total gravitational time delay of two-way time synchronization can be expressed as:

$$\begin{aligned} \delta^{grav} &= \left(\delta_{AB}^{grav}(T_0 - \frac{\rho_{AB}}{c}, T_0) - \delta_{BA}^{grav}(T_0 - \frac{\rho_{BA}}{c}, T_0)\right) \\ &= \frac{2GM}{c^3}ln\left(\frac{r_A(T_0 - \frac{\rho_{AB}}{c}) + r_B(T_0) + d_{AB}(T_0 - \frac{\rho_{AB}}{c}, T_0)}{r_A(T_0 - \frac{\rho_{AB}}{c}) + r_B(T_0) - d_{AB}(T_0 - \frac{\rho_{AB}}{c}, T_0)}\right) \\ &\quad - \frac{2GM}{c^3}ln\left(\frac{r_A(T_0) + r_B(T_0 - \frac{\rho_{BA}}{c}) + d_{BA}(T_0 - \frac{\rho_{BA}}{c}, T_0)}{r_A(T_0) + r_B(T_0 - \frac{\rho_{BA}}{c}) - d_{BA}(T_0 - \frac{\rho_{BA}}{c}, T_0)}\right) \end{aligned} \tag{12}$$

Relating the Equations (9) and (12) to Equation (3), the relativistic effect on satellite-ground two-way time synchronization can be accurately eliminated.

4. Simulation and Discussion

To verify the methods of time synchronization and correction of relativistic effects, a simulation platform has been developed using Matlab, including two parts: one is the data generation module, and the other is the performance evaluation module, as shown in Figure 3.
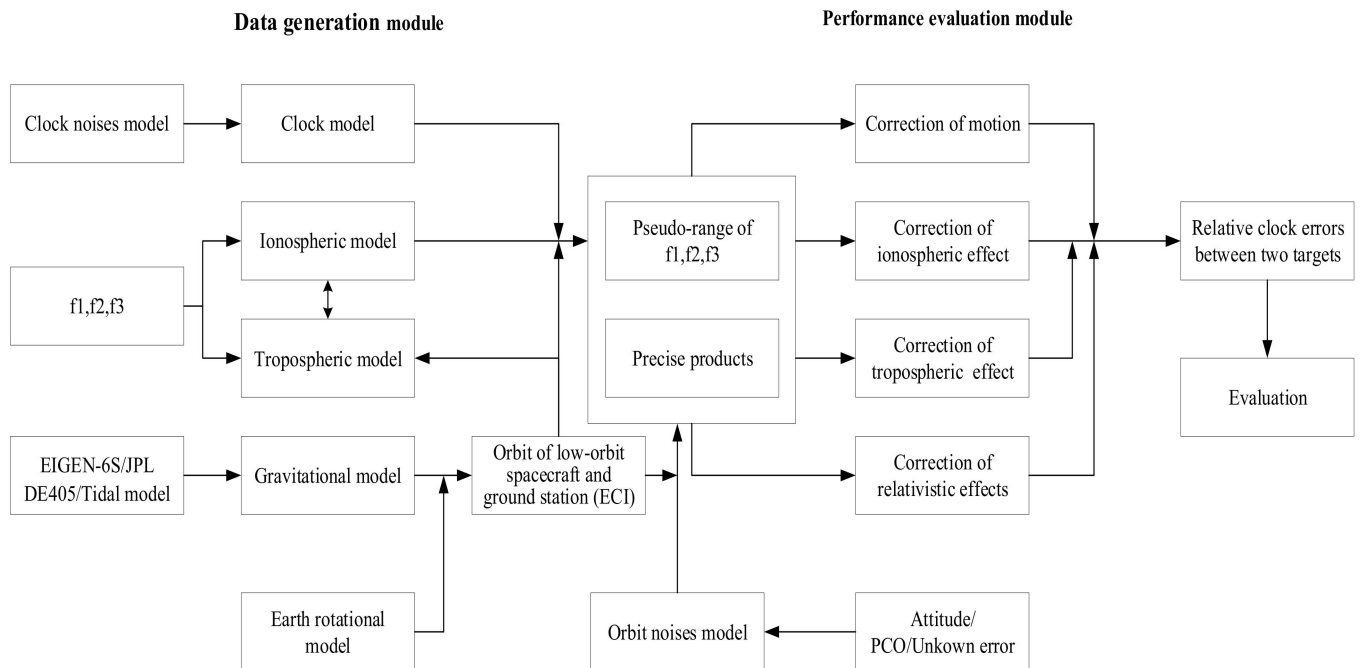

Figure 3. Simulation platform.

4.1. Data Generation

A low-orbit satellite trajectory (height of ~400 km) is simulated (Kepler orbit) by flying in an orbit with an inclination of approximately 45° [28]. In order to obtain the accurate satellite and ground station orbit information, we have fully considered a variety of main perturbation force models when generating simulation orbits (see Figure 3), e.g., Earth Gravity Model (EIGEN-6S), N-body Gravity Model (JPL DE-405), Tidal Model (FES-2004), etc. A high-precision earth rotation model must be adopted. The ground station is located in Xi'an, China. To nullify the Sagnac effect, the ECEF coordinates of the ground station and spacecraft are converted to ECI coordinates through the Earth orientation parameters (EOPs) file of International Earth Rotation Service (IERS) (https://www.iers.org/IERS). An ultrahigh precise atomic clock was employed onboard the low-orbit satellite, and the stability of the clock was set to 8E-18@1day. Because of the high-stability clock, the noise of the clock contributes little to the total errors of the transfer link, and it can almost be ignored. Using tri-frequency signals (20 GHz~40 GHz) to generate simulated pseudoranges, the involved errors include orbit error, clock error, ionospheric error, tropospheric error, and relativistic error. The fact of satellite-to-ground coverage shows the actual situation of satellite-ground communication [29], which is one of the important factors for realizing simulation. Table 3 shows the fact of the simulated low-orbit spacecraft link to Xi'an ground station (visibility results in one day using STK software), about 6 visible arcs per day while the low-orbit spacecraft pass over the ground station. Owing to the limitation of the payload's antenna pointing angle, each pass over the ground station can only observe approximately 300 s. We use the data simulation platform to generate 300s tri-frequency pseudorange data, as shown in Figure 4.

The pseudoranges of pair links with f1 and f2 can be used to decouple the relative clock between the satellite and ground station, and the downlink pseudoranges of f1 and f3 can be used to obtain the slant total electron content (STEC) and reduce the effects

of the ionosphere and troposphere. Figure 5 shows the different contributions in the pseudoranges. All of the contributions in the one-way transfer are greater than 10 ps, and they cannot be neglected for the ps-level time synchronization. In this paper, we mainly focus on using simulation data to verify the accuracy of the relativistic effect correction method and the realization of the satellite-ground two-way time synchronization method. Thus, it is possible to verify the relativistic correction algorithm without considering other errors except the relativistic error, and then verify the accuracy of the two-way time synchronization method while considering all effects.

Table 3. Visibility results in one day.

| Visible Arc Num.	Start Time (EpSec)	End Time (EpSec)	Duration (s)
1	1009.872	1280.094	270.222
2	6899.775	7244.119	344.344
3	67,539.405	67,797.561	258.156
4	73,389.376	73,745.408	356.032
5	79,379.406	79,631.930	252.524
6	85,326.710	85,590.520	263.810
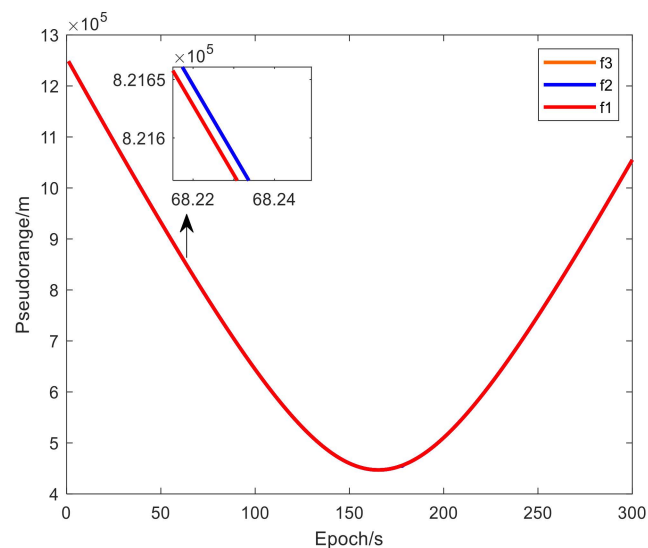
Figure 4. Pseudo-range data obtained by simulation.

4.2. Validating the Methods with Simulated Data

From Equations (7)–(10), to reduce the relativistic effects, we adopt the precise products [30] (orbit product and clock product) and the correction model to calculate the approximate value of the relativistic errors. Therefore, the correction accuracy of the model in Section 3 depends on the product accuracy and the perturbation force model of the spacecraft. To achieve ps-level time synchronization, additional perturbation force inputs are needed, considering the nonspherical gravitation (J_2 and others). On this basis, the orbit errors from the orbit product will become the biggest obstacle to correct the relativistic errors. The position vector of the spacecraft can be obtained by post-processing of the data from receivers [31], but the final results of the orbit product are coupled with the attitude error, phase center calibration error, and precise orbit determination (POD) error of the spacecraft [20].

In engineering, corresponding indices are proposed for these errors. We take poor indexes (0.02° attitude error, 2 mm phase center calibration error and 10 cm POD error) as a reference standard, which can be easily achieved. A less quantitative (and less absolute) criterion is the absence of a notable signature in the residuals: most of the time we expect

the spread to be uniform across the pass, and any visible pattern should be investigated as a possible consequence of implementation problems [32].
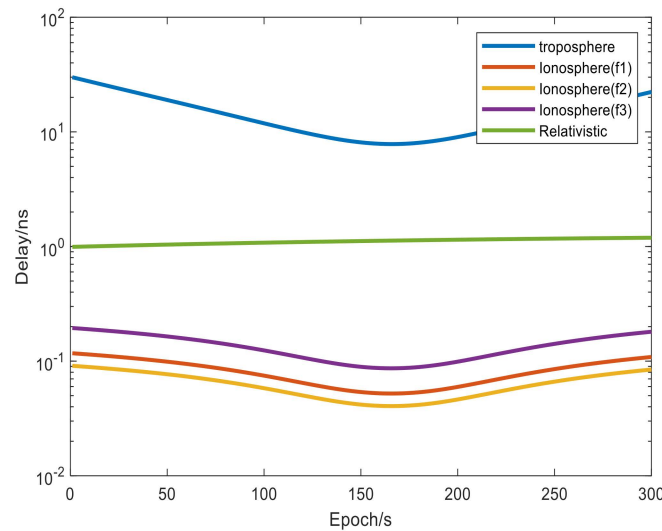

Figure 5. Contribution of atmospheric and relativistic delays in the simulated pseudorange of the f1/f2/f3 signal (absolute values).

When Figure 6a–f is examined, it can be seen that the residuals obtained by the relativistic error correction method in Section 3 were determined precisely. Here, a relativistic correction solution means that the accuracy (RMS, root mean square) is better than 1 ps in periodic relativity correction and 3×10^{-12} ps in gravitational time delay correction. Furthermore, we study the influence of one error on the correction of the relativistic errors with the condition of two errors unchanged (the constant indexes are $0.02°$ for attitude error, 2 mm for phase center calibration error and 10 cm for POD error). As a result, the RMS of the periodic relativity correction residual of different attitude errors, different phase center calibration errors, and different POD errors are approximately 0.52–0.55 ps, 0.40–0.60ps, and 0.42–0.70 ps, respectively, and the RMS of the gravitational time delay correction residual of different attitude errors, different phase center calibration errors, and POD errors are approximately 2×10^{-12}–2.6×10^{-12}, 1.6×10^{-12}–2.4×10^{-12}, and 1.6×10^{-12}–2.9×10^{-12} ns, respectively. Then, the influence of orbit errors on the accuracy of relativity correction can be roughly estimated and is shown in Table 4.

Table 4. The effect of comprehensive error factors on the correction of total relativistic effects (including attitude error, phase center calibration error and POD error).

	Attitude Error	Phase Center Calibration Error	POD Error
RMS of residual	0.02 ps–0.03 ps	0.1 ps–0.2 ps	0.2 ps–0.3 ps

When Figure 6 is examined together with Table 4, it can be seen that the effect of orbit error factors on the gravitational time delay correction is almost negligible. The effect of three errors (attitude error, phase center calibration error, and POD error) on total relativistic correction can range from 0.02–0.03 ps, 0.1–0.2 ps, and 0.2–0.3 ps, respectively. For ps-level time synchronization, the attitude error can be ignored, but the phase center calibration error and POD error must be considered, and the error of periodic relativity must be corrected by the precise model proposed in the paper.
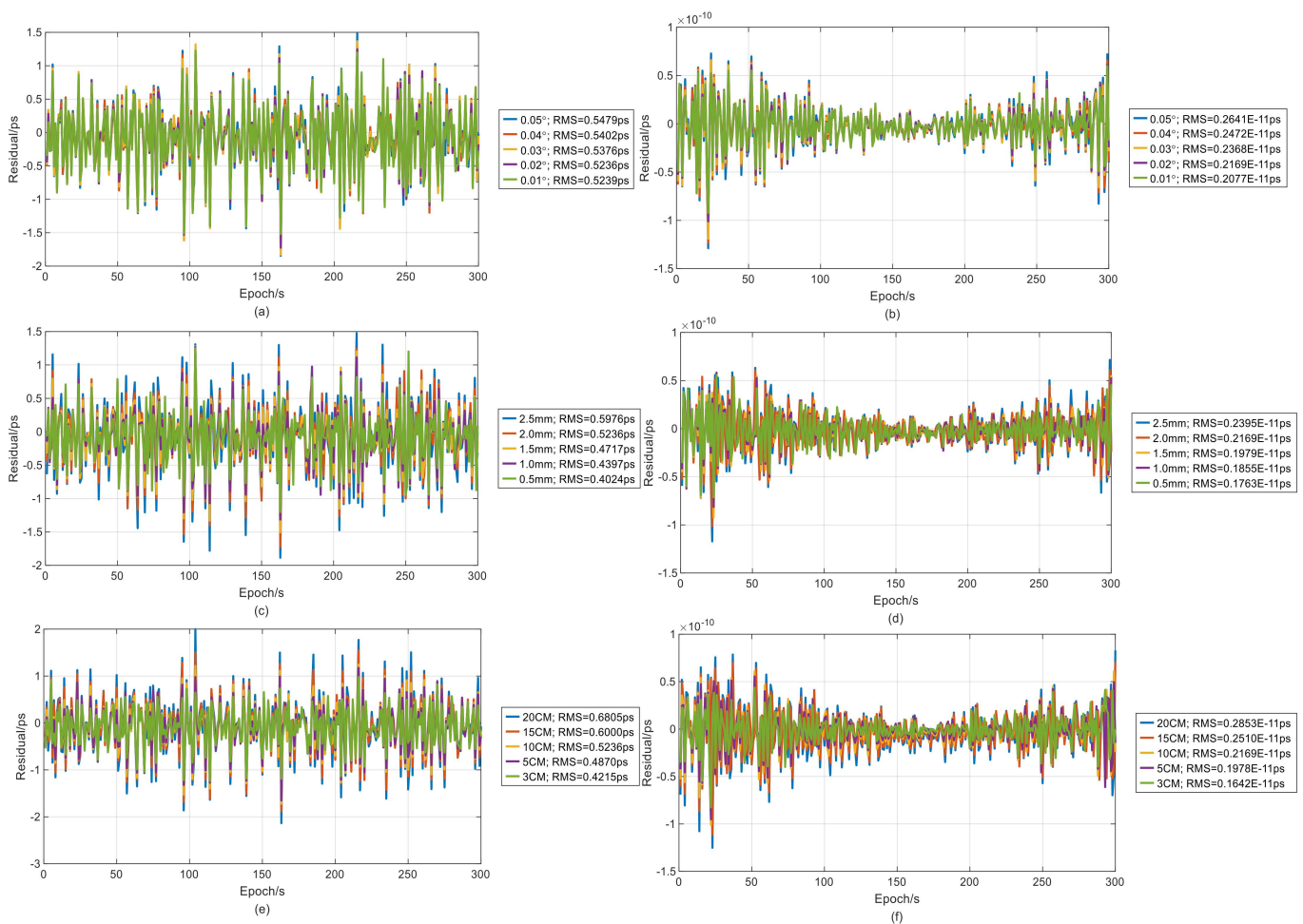
Figure 6. The influence of different orbit errors on the accuracy of the relativistic correction model. (**a**,**b**) The influence of different attitude errors on periodic relativity and gravitational time delay correction, respectively. (**c**,**d**) The influence of different phase center calibration errors on periodic relativity and gravitational time delay correction, respectively. (**e**,**f**) The influence of different POD errors on periodic relativity and gravitational time delay correction, respectively.

The correction of relativistic effects is closely related to the POD error, attitude error, and phase center calibration error. When the attitude error is no more than 0.02°, the phase center calibration error is less than 2 mm, the POD error is better than 10 cm, and other errors (ignoring the hardware error) in the process of time synchronization are fully considered. Then, the relativistic correction method in this paper is used to process and calibrate the simulated data, and the relative clock error between the spacecraft and the ground station is further calculated by the two-way time synchronization method. Through the quadratic fitting of the relative clock error, the performance of time synchronization can be evaluated [33]. The time synchronization performance of the satellite-ground MWL is shown in Figure 7. The peak-to peak value of the time synchronization residual is no more than 2 ps and the accuracy (RMS) of satellite-ground time synchronization is better than 0.6 ps.
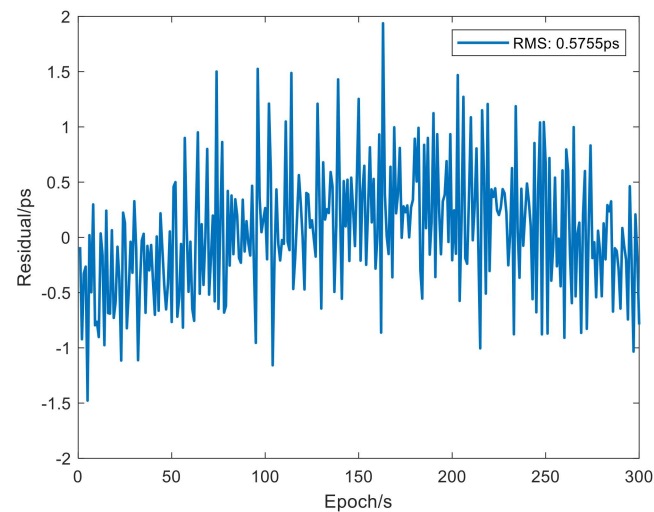
Figure 7. Satelliteground time synchronization residual. (After calculating the relative clock error between the satellite and the ground, the quadratic fitting model is used to fit the clock error, the residual after fitting represents the time synchronization residual, and the root mean square (RMS) of the residual represents the accuracy of time synchronization).

5. Conclusions

In this work, we studied a precise method of time synchronization between a spacecraft and a ground station, to achieve ps-level time synchronization accuracy. In this method, a high-precision relativity correction was first applied to accurately estimate the relativistic errors contained in the two-way link. To validate the time synchronization method and the relativity correction method, we built a simulation platform where we take the real situation of the earth and the signal propagation, considering all errors involved in the process of signal propagation. It can generate two-way ranging data and verify the methods by the simulated data. When the attitude error, phase center calibration error, and POD error are taken into consideration, the impact of attitude error can be almost negligible, the effect of phase center calibration error and POD error on relativistic correction can range from 0.1–0.2 ps and 0.2–0.3 ps, respectively. As an example of the application of these methods we have used them to demonstrate that typical low-orbit spacecraft orbitography errors (attitude error of ~0.02°, phase center calibration error of ~2 mm, POD error of ~10 cm) affect the two-way time synchronization below its performance specifications (1 ps), and thus can reach the expected accuracy requirements on the science objectives that depend on that performance. Final methods development will occur during the remaining phases. As soon as the hardware error is confirmed and data schemes freeze, we will need to fine-tune our methods (including the tri-frequency time synchronization method and error correction method) and adapt our flow to possible deviations with respect to the present situation or assumptions.

Author Contributions: Conceptualization, Y.G. and Y.B.; data curation, Y.G.; formal analysis, Y.G. and S.G.; funding acquisition, Y.B., S.G., X.L. and S.Z.; methodology, Y.G.; project administration, Y.G., Z.P. and Z.H.; resources, S.G., D.Z., X.L. and S.Z.; software, Y.G.; validation, Y.G. and Z.P.; writing—original draft, Y.G., writing—review and editing, Y.G. and Y.B. All authors have read and agreed to the published version of the manuscript.

Institutional Review Board Statement: Not applicable.

Informed Consent Statement: Not applicable.

Abbreviations

Abbreviation	Definition
POD	precise orbit determination
PNT	Positioning, navigation and timing
GNSS	Global navigation satellite system
BDS-3	BeiDou-3 navigation system
ESA	European Space Agency
ISS	International Space Station
MWL	Microwave link
CSS	Chinese Space Station
GSLs	Satellite-ground links
ISLs	Inter-satellite links
LEO	Low-orbit earth orbit
TDMA	Time division multiple access
TWSTFT	Two-way Satellite Time and Frequency Transfer
ECI	Earth-centered inertial
NFO	Nominal frequency offset
EOPs	Earth orientation parameters
IERS	International Earth Rotation Service
STEC	Slant total electron content
PCO	Phase center offset
RMS	Root mean square

References

1. Mehlstäubler, T.E.; Grosche, G.; Lisdat, C.; Schmidt, P.O.; Denker, H. Atomic clocks for geodesy. *Rep. Prog. Phys.* **2018**, *81*, 064401. [CrossRef]
2. Pan, J.; Hu, X.; Zhou, S.; Tang, C.; Guo, R.; Zhu, L.; Tang, G.; Hu, G. Time synchronization of new-generation BDS satellites using inter-satellite link measurements. *Adv. Space Res.* **2018**, *61*, 145–153. [CrossRef]
3. Tang, G.; Yang, W.; Su, R.; Xia, A. Time Synchronization Method base on Combined Satellite-Ground and Inter-satellite Observation. *Wuhan Daxue Xuebao Geomat. Inf. Sci. Wuhan Univ.* **2018**, *43*, 183–187.
4. Delva, P.; Meynadier, F.; Le Poncin-Lafitte, C.; Laurent, P.; Wolf, P. Time and frequency transfer with a MicroWave Link in the ACES/PHARAO mission. In Proceedings of the 2012 European Frequency and Time Forum, Gothenburg, Sweden, 23–27 April 2012; pp. 28–35.
5. Meynadier, F.; Delva, P.; Le Poncin Lafitte, C.; Guerlin, C.; Laurent, P.; Wolf, P. ACES Micro-wave link data analysis: Status update. In Proceedings of the Journées Systèmes De Référence Spatio Temporels Scientific Developments from Highly Accurate Space Time Reference Systems, Paris, France, 16–18 September 2013; pp. 134–135.
6. Cacciapuoti, L.; Armano, M.; Much, R.; Sy, O.; Helm, A.; Hess, M.P.; Kehrer, J.; Koller, S.; Niedermaier, T.; Esnault, F.; et al. Testing gravity with cold-atom clocks in space. *Eur. Phys. J. D* **2020**, *74*, 164. [CrossRef]
7. Much, R.; Daganzo, E.; Feltham, S.; Nasca, R.; Hess, M.P.; Stringhetti, L.; Cacciapuoti, L.; Salomon, C. Status of the ACES mission. In Proceedings of the 2009 IEEE International Frequency Control Symposium Joint with the 22nd European Frequency and Time Forum, Besancon, France, 20–24 April 2009; pp. 199–204.
8. Zhang, X. System design and key technologies of high accuracy time and frequency microwave link for spaces station. *Telecommun. Eng.* **2017**, *57*, 407–411.
9. Sun, W. Satellite in low orbit(champ, grace, goce) and high precision earth gravity field: The latest progress of satellite gravity geodesy and its great influence on geoscience. *Crustal Deform. Earthq.* **2002**, *22*, 92–100.
10. Edward, A.L. A Comparison of Relativistic Impacts on Satellite Timekeeping for Various Orbits. In Proceedings of the 52nd Annual Precise Time and Time Interval Systems and Applications Meeting, Virtual online, 25–28 January 2021; pp. 326–337.

11. Xie, P.; Zhang, Z.; Zhang, J. Topology transformation based on time division: An improved inter-satellite link structure. In Proceedings of the Chinese Control and Decision Conference (CCDC), Shenyang, China, 9–11 June 2018; pp. 3761–3766.

12. Hess, M.P.; Kehrer, J.; Kufner, M.; Durand, S.; Hejc, G.; Frühauf, H.; Cacciapuoti, L. ACES MWL status and test results. In Proceedings of the Joint Conference of the IEEE International Frequency Control and the European Frequency and Time Forum (FCS) Proceedings, San Francisco, CA, USA, 2–5 May 2011; pp. 1–8.

13. Hanson, D.W. Fundamentals of two-way time transfers by satellite. In Proceedings of the 43rd Annual Symposium on Frequency Control, Denver, CO, USA, 31 May–2 June 1989; pp. 174–178. [CrossRef]

14. Xie, X.; Geng, T.; Zhao, Q.; Cai, H.; Zhang, F.; Wang, X.; Meng, Y. Precise orbit determination for BDS-3 satellites using satellite-ground and inter-satellite link observations. *GPS Solut.* **2019**, *23*, 40. [CrossRef]

15. Ruan, R.; Jia, X.; Feng, L.; Zhu, J.; Wei, Z. Orbit determination and time synchronization for BDS-3 satellites with raw inter-satellite link ranging observations. *Satell. Navig.* **2020**, *1*, 8. [CrossRef]

16. Hobiger, T.; Piester, D.; Baron, P. A correction model of dispersive troposphere delays for the ACES microwave link. *Radio Sci.* **2013**, *48*, 131–142. [CrossRef]

17. Sun, X.; Shen, W.B.; Shen, Z.; Cai, C.; Xu, W.; Zhang, P. Formulation to test gravitational redshift based on the tri-frequency combination of ACES frequency links. *Eur. Phys. J. C* **2021**, *81*, 634. [CrossRef]

18. Yang, Y.; Yang, Y.; Hu, X.; Tang, C.; Guo, R.; Zhou, Z.; Xu, J.; Pan, J.; Su, M. BeiDou-3 broadcast clock estimation by integration of observations of regional tracking stations and inter-satellite links. *GPS Solut.* **2021**, *25*, 57. [CrossRef]

19. Xie, X.; Geng, T.; Zhao, Q.; Lv, Y.; Liu, J. Orbit and clock analysis of BDS-3 satellites using inter-satellite link observations. *J. Geod.* **2020**, *94*, 64. [CrossRef]

20. Guo, Y.; Bai, Y.; Gao, S.; Pan, Z.; Han, Z.; Gao, Y.; Lu, X. A SatelliteGround Precise Time Synchronization Method and Analysis on Time Delay Error Caused by Motion. In Proceedings of the China Satellite Navigation Conference (CSNC) 2021 Proceedings, Nanchang, China, 26–28 May 2021; Volume 3, pp. 158–171.

21. Han, C.; Cai, Z. Relativistic effects to the onboard BeiDou satellite clocks. *Navigation* **2019**, *66*, 49–53. [CrossRef]

22. Hećimović, Ž. Relativistic effects on satellite navigation. *Teh. Vjesn.* **2013**, *20*, 195–203.

23. Larson, K.M.; Ashby, N.; Hackman, C.; Bertiger, W. An assessment of relativistic effects for low Earth orbiters: The GRACE satellites. *Metrologia* **2007**, *44*, 484–490. [CrossRef]

24. Sun, L.; Gao, S.; Yang, J.; Xiao, F.; Fang, Y.; Feng, S. Relativistic Effect in the Two-Way Time Comparison Between Navigation Satellites. In Proceedings of the China Satellite Navigation Conference (CSNC) 2021 Proceedings, Nanchang, China, 26–28 May 2021; Volume 3, pp. 95–104.

25. Chen, H.; Wu, H.; Zhou, M.; Qi, J. *Orbit Engineering Application and STK Simulation for Microsatellite*; Science Press: Beijing, China, 2016; p. 71.

26. Bisnath, S. Precise Orbit Determination of Low Earth Orbiters with a Single GPS Receiver-Based, Geometric Strategy. 2004, p. 8. Available online: https://unbscholar.lib.unb.ca/islandora/object/unbscholar%3A8487 (accessed on 1 October 2021).

27. Kaula, W.M. *Theory of Satellite Geodesy*; Blaisdell Publishing Company, Dover Publications: New York, NY, USA, 1966; p. 45.

28. Shao, K.; Gu, D.; Ju, B.; Wang, W.; Wang, Z. Analysis of Tiangong-2 orbit determination and prediction using onboard dual-frequency GNSS data. *GPS Solut.* **2020**, *24*, 11. [CrossRef]

29. Chronopoulos, S.K.; Angelis, C.T.; Koumasis, A.; Drakou, P. Satellite Coverage Analysis for the Investigation of Real-Time Communication in Selected Areas. *WSEAS Trans. Commun.* **2006**, *5*, 1965–1972.

30. Cao, X.; Shen, F.; Zhang, S.; Li, J. Time delay bias between the second and third generation of BeiDou Navigation Satellite System and its effect on precise point positioning. *Measurement* **2020**, *168*, 108346. [CrossRef]

31. Wen, X.; Hao, J.; Hu, X.; Tang, C.; Wang, D.; Chen, L.; Chang, Z.; Zhu, L.; Wu, S.; Li, X. Feasibility Analysis of Time Synchronization of Beidou Satellite Using Inter-Satellite Observation Data. *J. Geod. Geodyn.* **2018**, *38*, 1274–1279.

32. Meynadier, F.; Delva, P.; le Poncin-Lafitte, C.; Guerlin, C.; Wolf, P. Atomic clock ensemble in space (ACES) data analysis. *Class. Quantum Gravity* **2018**, *35*, 035018. [CrossRef]

33. Yang, Y. *Research on the Method and Theory of BDS-3 PNT Service SIS Accuracy Improvement Using Inter-Satellite Link*; Force Information Engineering University: Zhengzhou, China, 2011.